

A disease mutation reveals a role for Na_v1.9 in acute itch

Juan Salvatierra, ... , Xinzhong Dong, Frank Bosmans

J Clin Invest. 2018. <https://doi.org/10.1172/JCI122481>.

Research Article

Neuroscience

Itch (pruritis) and pain represent two distinct sensory modalities; yet both have evolved to alert us to potentially harmful external stimuli. Compared with pain, our understanding of itch is still nascent. Here, we report a new clinical case of debilitating itch and altered pain perception resulting from the heterozygous de novo p.L811P gain-of-function mutation in Na_v1.9, a voltage-gated sodium (Na_v) channel subtype that relays sensory information from the periphery to the spine. To investigate the role of Na_v1.9 in itch, we developed a mouse line in which the channel is N-terminally tagged with a fluorescent protein, thereby enabling the reliable identification and biophysical characterization of Na_v1.9-expressing neurons. We also assessed Na_v1.9 involvement in itch by using a newly created Na_v1.9^{-/-} and Na_v1.9^{L799P/WT} mouse model. We found that Na_v1.9 is expressed in a subset of nonmyelinated, nonpeptidergic small-diameter dorsal root ganglia (DRGs). In WT DRGs, but not those of Na_v1.9^{-/-} mice, pruritogens altered action potential parameters and Na_v channel gating properties. Additionally, Na_v1.9^{-/-} mice exhibited a strong reduction in acute scratching behavior in response to pruritogens, whereas Na_v1.9^{L799P/WT} mice displayed increased spontaneous scratching. Altogether, our data suggest an important contribution of Na_v1.9 to itch signaling.

Find the latest version:

<https://jci.me/122481/pdf>



A disease mutation reveals a role for Na_v1.9 in acute itch

Juan Salvatierra,¹ Marcelo Diaz-Bustamante,¹ James Meixiong,² Elaine Tierney,³ Xinzhong Dong,^{2,4} and Frank Bosmans^{1,2,5}

¹Department of Physiology, ²Solomon H. Snyder Department of Neuroscience, ³Department of Psychiatry and Behavioral Sciences, and ⁴Howard Hughes Medical Institute, Johns Hopkins University School of Medicine, Baltimore, Maryland, USA. ⁵Department of Basic and Applied Medical Sciences, Ghent University, Ghent, Belgium.

Itch (pruritis) and pain represent two distinct sensory modalities; yet both have evolved to alert us to potentially harmful external stimuli. Compared with pain, our understanding of itch is still nascent. Here, we report a new clinical case of debilitating itch and altered pain perception resulting from the heterozygous de novo p.L811P gain-of-function mutation in Na_v1.9, a voltage-gated sodium (Na_v) channel subtype that relays sensory information from the periphery to the spine. To investigate the role of Na_v1.9 in itch, we developed a mouse line in which the channel is N-terminally tagged with a fluorescent protein, thereby enabling the reliable identification and biophysical characterization of Na_v1.9-expressing neurons. We also assessed Na_v1.9 involvement in itch by using a newly created Na_v1.9^{-/-} and Na_v1.9^{L799P/WT} mouse model. We found that Na_v1.9 is expressed in a subset of nonmyelinated, nonpeptidergic small-diameter dorsal root ganglia (DRGs). In WT DRGs, but not those of Na_v1.9^{-/-} mice, pruritogens altered action potential parameters and Na_v channel gating properties. Additionally, Na_v1.9^{-/-} mice exhibited a strong reduction in acute scratching behavior in response to pruritogens, whereas Na_v1.9^{L799P/WT} mice displayed increased spontaneous scratching. Altogether, our data suggest an important contribution of Na_v1.9 to itch signaling.

Introduction

The somatosensory nervous system detects sensory modalities such as pain, itch, and temperature sensitivity and transfers them from the periphery to the spinal cord and eventually to the sensory cortex in the brain (1). Of these signals, itch (pruritis) has evolved to alert us to potentially dangerous external stimuli (2, 3). Although acute itch may guard against environmental threats, pathological itch is a distressing physical sensation and can dramatically affect quality of life. Yet, compared with other sensory modalities, itch is much less understood. Histamine was the first compound discovered to elicit itch by activating a subset of peripheral sensory neurons (pruriceptors) (4–6). Later, additional receptors were identified as key players in mediating itch sensation. The discovery of Mas-related G protein-coupled receptors (Mrgprs) as critical contributors to itch helped identify potential itch-selective neurons (7). The 4 families of histamine-independent Mrgprs (MrgprA–D) can be activated by pruritic compounds such as chloroquine (CQ) and BAM8-22 and are expressed in trigeminal ganglia and dorsal root ganglia (DRGs) (8–10). Although these receptors and others have been established as initial detectors of pruritic stimuli (11–16), the downstream mechanisms involved in mediating itch are still poorly understood.

Although voltage-gated Na⁺ channels (Na_v1.1–Na_v1.9) are critical for the propagation of action potentials (APs) (17) in sensory neurons, little is known about how they contribute to the trans-

mission of pruritic stimuli. Specifically, the relationship between Na_v1.7, Na_v1.8, and Na_v1.9 and pain has been studied extensively, with knockout mouse models for all 3 channels showing effects in various pain assays (18–27). However, the contribution of these and other Na_v channel subtypes to itch has yet to be explored.

Here, we report a new clinical case of unbearable itch and distorted pain sensation stemming from the heterozygous de novo p.L811P mutation in Na_v1.9 channels, encoded by the *SCN11A* gene. This mutation was previously published in relation to several cases of complete insensitivity to pain in which abnormal Na_v1.9 function was thought to result in nociceptor depolarization and subsequent conduction block (22, 28). Although there is a consensus that Na_v1.9 contributes to pain (20, 29, 30), the role of this Na_v channel subtype and the p.L811P^{+/-} mutation in itch is unknown (31). Compared with other Na_v channel subtypes, the expression patterns, functional properties, and pharmacological sensitivities of Na_v1.9 are less defined. To investigate the role of Na_v1.9 in itch, we assessed its functional role in new mouse models in which channel expression was spatiotemporally manipulated. We also tagged Na_v1.9 with a fluorescent reporter to facilitate reliable identification and biophysical characterization of Na_v1.9-expressing cells. We found that the channel is present in a subset of nonmyelinated, nonpeptidergic small-diameter DRGs. In WT DRGs but not in Na_v1.9^{-/-} mice, pruritogens altered AP parameters and Na_v channel gating properties. Compared with control animals, Na_v1.9^{-/-} mice displayed reduced scratching behavior upon application of histamine, CQ, and BAM8-22. Combined with the observation that disease-related L799P/WT mice exhibited amplified scratching behavior in rest conditions, our data provide compelling evidence for Na_v1.9 participation in itch.

Conflict of interest: The authors have declared that no conflict of interest exists.

License: Copyright 2018, American Society for Clinical Investigation.

Submitted: May 29, 2018; **Accepted:** September 20, 2018.

Reference information: *J Clin Invest*. <https://doi.org/10.1172/JCI122481>.

Results

A newly identified $Na_v1.9^{L799P/WT}$ patient. Whole-exome sequencing uncovered the de novo p.L811P (c.T2432C) mutation in $Na_v1.9$ in a female patient reporting severe pruritus without a family history. In addition to itch, the patient reported a partial loss-of-pain sensation with remaining back, neck, and side pain. Past medical history included fractures in her lower extremities with little trauma, diurnal and nocturnal enuresis, constipation, intermittent diarrhea, developmental delay, heterotrophic ossification with bilateral hip disease, scoliosis, hyperhidrosis, asthma, eczema, gastroesophageal reflux, hypoglycemia, vitamin D deficiency, headaches, and picking of the skin on her fingers.

Regarding itch experienced, the patient reported that itch was worse at night, even in the absence of topical skin pathology such as eczema, and that itching, tingling, sweating, and movement of lower extremities commonly prevented her from falling asleep. The patient had excoriations and marks on her legs from scratching, and her fingers bled from picking pieces of skin. She used compression bandages and pressed on her lower extremities to lessen itching sensations and wore mitts to bed to prevent scratching herself while asleep. The patient reported no itch relief from diazepam or oxycodone and only a minor benefit from diphenhydramine and acetaminophen. Physical examination revealed that the patient had a lack of position sense in the toes, had distal movement sense in both ankles, and detected von Frey 0.07 g filament on the dorsum of her feet. Further examination with a pin showed that she had decreased sensation bilaterally that was dull initially but turned painful after repeated touch. The patient was also diagnosed with restless legs syndrome (RLS) and anxiety disorder not otherwise specified. She was treated with cyproheptadine after reporting partial improvement of itch with diphenhydramine. Gabapentin was added to her treatment because of the reported decrease in discomfort in individuals with small-fiber neuropathy (32) and the reduction in lower-extremity movements in patients with RLS (33). Subsequently, she no longer damaged her lower-extremity skin by rubbing or scratching, and her evening discomfort lessened drastically, allowing lesions to heal. After healing, severe wounds from scratching left marks that resembled bruising (Figure 1A, arrows). The observation that no other mutations were found in patients with the $Na_v1.9^{L811P}$ mutation, and that most reported patients with this mutation complained of severe pruritus (31), suggests an important contribution of $Na_v1.9$ to itch.

Generation and characterization of an sfGFP-tagged $Na_v1.9$ mouse line. To determine the expression pattern of $Na_v1.9$, we used a mouse line in which the channel was fused to a fluorescent reporter. To limit impact on $Na_v1.9$ function and expression, we (a) used superfolder green fluorescent protein (sfGFP), a generation of GFP with enhanced folding kinetics (34); (b) targeted the N-terminus of the channel for sfGFP fusion (17, 35); and (c) codon-optimized (36) sfGFP. Using the flexible accelerated Neo-STOP tetracycline-inducible (FAST) technique (37), we inserted sfGFP immediately after the endogenous start codon (Figure 1B). The original knock-in cassette contained a construct (loxP-FRT-Neo-STOP-FRT-tetO-loxP) that led to a global $Na_v1.9$ knockout phenotype ($Na_v1.9^{-/-}$ FAST mice). This strain had the additional benefit of being capable of (a) tetracycline-controlled transacti-

vator-mediated (tTA-mediated) overexpression and (b) tetracycline-controlled transcriptional silencer-mediated (tTS-mediated) conditional knockdown (Figure 1B).

By crossing sfGFP- $Na_v1.9$ FAST mice (C57BL/6J) with a global Cre mouse (B6.C-Tg^(CMV-cre)1Cgn; The Jackson Laboratory), we obtained a line in which endogenous $Na_v1.9$ was N-terminally fused to sfGFP. As seen in Figure 1C, a subset of dissociated DRGs displayed robust fluorescence signal that overlapped with a GFP antibody, whereas WT tissue only showed weak background fluorescence. Biochemical analysis of DRGs showed the presence of a GFP⁺ band at the appropriate size for sfGFP-tagged $Na_v1.9$, which was not observed in either WT or FAST cassette-containing mouse DRGs (Figure 1D). Correspondingly, quantitative reverse transcriptase PCR (RT-qPCR) did not detect $Na_v1.9$ RNA in DRGs of FAST mice. Blotting for GFP and then stripping and reprobing of the Western blot with an $Na_v1.9$ antibody (38) revealed a positive band in both DRGs and trigeminal ganglia. Aside from these tissues, $Na_v1.9$ expression was not observed in the brain or other major organs (Figure 1E).

After confirming expression of fluorescence, we next sought to determine whether the gating properties of sfGFP-tagged $Na_v1.9$ were altered when compared with nontagged $Na_v1.9$. Patch-clamp recordings from fluorescent sensory neurons in the presence of tetrodotoxin (TTX) and CsF in the patch pipette revealed a functional sfGFP- $Na_v1.9$ channel with WT gating behavior and kinetics as reported in the literature (refs. 21, 22, 24, 39–43; and Supplemental Figure 1; supplemental material available online with this article; <https://doi.org/10.1172/JCI122481DS1>).

To further validate proper channel function, we constructed mouse WT $Na_v1.9$ and sfGFP- $Na_v1.9$ stable rodent DRG-derived ND7/23 cell lines by combining the FLP recombination target-based (FRT-based) FLP-In system (Thermo Fisher Scientific) with intron-mediated enhancement of gene expression, a technique that leads to increased accumulation of mRNA and protein relative to unaltered cDNA (44). An additional benefit of this approach was the reduction of unwanted rearrangement events when propagating Na_v channel cDNA in bacteria. The mouse *SCN11a* gene is encoded by 24 exons with known exon/intron boundaries (45). Although we did not obtain sufficient expression with mouse cDNA lacking an endogenous intron or with the addition of C-terminal GFP (46), we consistently saw $Na_v1.9$ current with cDNA containing intron 2 that increased after differentiation of the ND7/23 cells in medium containing NGF (100 ng/ml) and 1% FBS (Figure 1, F and G). RT-PCR and sequencing confirmed the correct excision of intron 2 to form mature channels (45). Patch-clamp recordings from these cells showed sfGFP- $Na_v1.9$ and WT channel currents with virtually identical gating properties and kinetics (Figure 1, H–J).

$Na_v1.9$ is predominantly expressed in nonmyelinated small-diameter DRGs. We exploited the sfGFP tag to determine $Na_v1.9$ expression in mouse DRG subtypes. Using IHC with a GFP antibody, we found that all sfGFP⁺ cells overlapped with peripherin, a marker for peripheral sensory neurons (Figure 2A). We also observed strong overlap between sfGFP and IB4 (Figure 2B; 86%) and c-Ret (Figure 2C; 89%), 2 markers for small-diameter, unmyelinated nonpeptidergic fibers. We detected a small portion of sfGFP⁺ cells that overlapped with calcitonin gene-related pep-

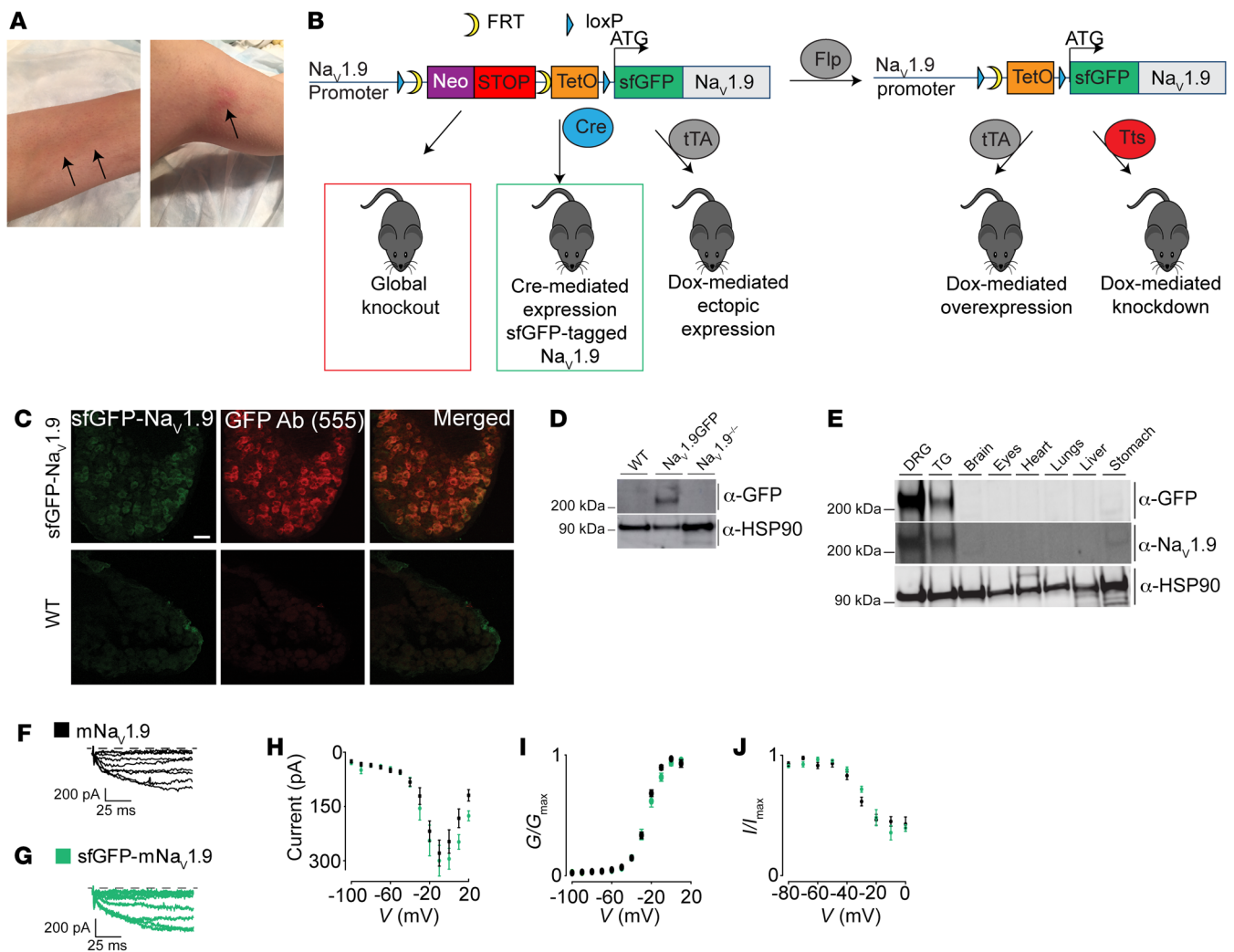


Figure 1. Generation and characterization of Na_v1.9 mouse lines. (A) After healing, wounds from scratching left marks that resembled bruising (black arrows) in the p.L811P patient. (B) Schematic diagram of the flexible accelerated Neo-STOP tetracycline-inducible (FAST) cassette illustrating the generation of global-knockout Na_v1.9 mice (red box) and Cre-mediated expression of sfGFP-tagged Na_v1.9 mice (green box). (C) A DRG section from an sfGFP-tagged Na_v1.9 (top) and a WT mouse (bottom) showing the overlap between endogenous fluorescent signal (green) and autofluorescence, followed by staining with an antibody against GFP (red). (D) Western blot of DRG tissue from a WT, an sfGFP-Na_v1.9, and an Na_v1.9^{-/-} mouse stained for GFP. An HSP90 antibody was used as a loading control. (E) Western blot of tissues taken from an sfGFP-Na_v1.9 mouse and stained for GFP, stripped, and reprobed for Na_v1.9 using a commercial antibody. An HSP90 antibody was used as a loading control. TG, trigeminal ganglia. (F and G) Representative current traces from ND7/23 cell lines expressing WT (black) or sfGFP-Na_v1.9 (green) channels. (H–J) Current-voltage (*I*-*V*) (H) and deduced conductance-voltage (*G*-*V*) (I) and steady-state inactivation (SSI) (J) relationships of WT (black) and sfGFP-Na_v1.9 (green). (*G*-*V*: WT-Na_v1.9 $V_{1/2} = -25.5 \pm 0.5$ mV, $n = 16$; GFP-Na_v1.9 $V_{1/2} = -24.0 \pm 0.2$ mV, $n = 11$, $P = 0.52$; SSI: WT-Na_v1.9 $V_{1/2} = -29.3 \pm 3.5$ mV, $n = 7$; GFP-Na_v1.9 $V_{1/2} = -26.6 \pm 1.7$ mV, $n = 7$, $P = 0.49$). Data are represented as mean \pm SEM. Scale bar: 50 μm.

tide (CGRP), indicating a subpopulation of Na_v1.9⁺ neurons that are peptidergic (Figure 2D; 12%). We rarely spotted commonality of Na_v1.9 with NF200, a marker for large-diameter neurons (Figure 2E; 1.5%). Na_v1.9 has been implicated in thermal hyperalgesia under inflammatory conditions (23, 25, 47), and we indeed found substantial overlap with TRPV1 (Figure 2F; 35%), a marker for thermosensitive nociceptor subgroups (48). However, these TRPV1⁺ cells had low Na_v1.9 expression (Figure 2F, arrowheads). Markedly, sfGFP⁺ DRGs showed little to no overlap with TRPV2 (Figure 2G; 5%). Finally, we did not observe Na_v1.9 in tyrosine hydroxylase-expressing cells (49), which have been implicated in allodynia (50) (Figure 2H; 0.7%). In line with previous reports,

we detected Na_v1.9 in small to medium-sized neurons, which make up most nociceptors and pruriceptors (Figure 2, I and J). In addition, we crossed our homozygous sfGFP-Na_v1.9 mice with Na_v1.8-Cre-tdTomato mice that express the Cre recombinase under control of the Na_v1.8 promoter to induce tdTomato fluorescent protein in Na_v1.8-expressing neurons (51). As a result, we found extensive expression overlap between Na_v1.8 and Na_v1.9 (Supplemental Figure 2A). We also explored Na_v1.9 expression in vagal ganglia responsible for transmitting stimuli from organs such as the heart, larynx, lungs, and alimentary tract to the central nervous system (1). Here, we found that all Na_v1.9⁺ neurons expressed the pan-neuronal marker PGP9.5 (Supplemental Fig-

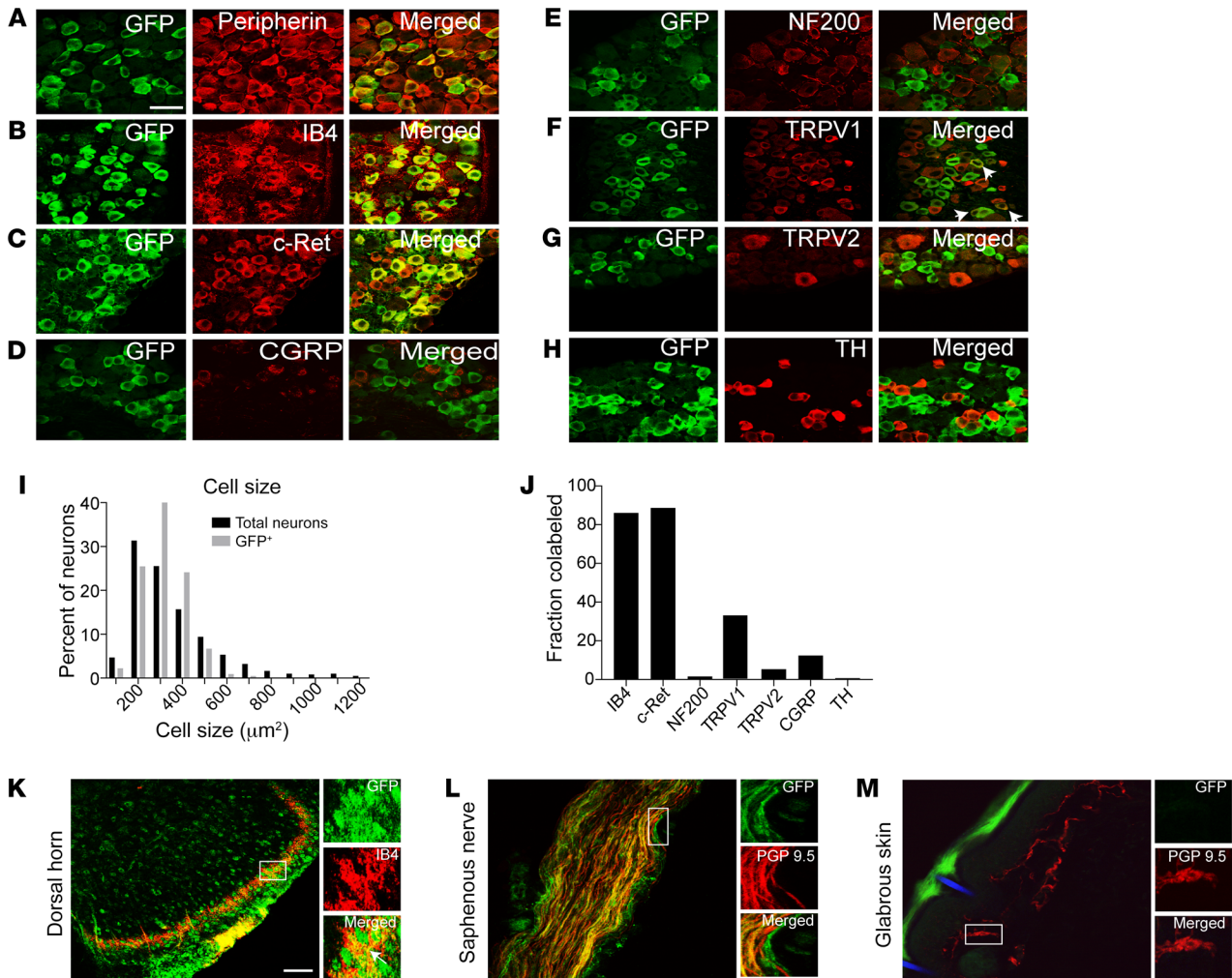


Figure 2. sfGFP- $\text{Na}_v1.9$ expression patterns. (A–H) DRG sections from sfGFP- $\text{Na}_v1.9$ mice stained for the indicated markers. TH, tyrosine hydroxylase. (I) Graph of cell area in DRGs with the total number of neurons by cell size (black bars), using the pan-neuronal marker PGP9.5, as well as the neurons positive for GFP staining (gray bars, $n \geq 200$ GFP⁺ neurons and $n \geq 600$ PGP9.5⁺). (J) Graph showing the fraction of neurons positive for the markers indicated that were also positive for GFP ($n \geq 200$ neurons). (K–M) Sections of the dorsal horn stained with GFP and IB4 (K), the saphenous nerve stained with GFP and PGP9.5 (L), and glabrous skin of the hind paw stained with GFP and PGP9.5 (M). Panels to the right of each image (K–M) show enlarged pictures of the corresponding section in the white box. Scale bars: 50 μm .

ure 2B) and detected extensive expression of $\text{Na}_v1.9$ in the jugular ganglia (Supplemental Figure 2C); however, we did not find cells with high levels of $\text{Na}_v1.9$ expression in the nodose ganglia (Supplemental Figure 2D). Finally, we determined $\text{Na}_v1.9$ expression at central and peripheral ends of the DRG. The fluorescent signal overlaps extensively with IB4 at the inner portion of layer II of the dorsal horn, where connecting interneurons may be involved in influencing pruritic circuits (52, 53) (Figure 2K). We also observed extensive fluorescence along the axon of the saphenous nerve (Figure 2L). Although we saw strong staining for PGP9.5, we could not detect significant sfGFP signal at the nerve terminals of either the glabrous skin or the hairy skin of the mouse hind paw in whole-mount skin preparations (Figure 2M and Supplemental Figure 2E).

$\text{Na}_v1.9$ expression in *MrgprA3/MrgprC11* neurons. The GPCRs *MrgprA3* and *MrgprC11* are expressed in a subpopulation of nociceptors linked to non-histamine-related itch (10). To examine whether $\text{Na}_v1.9$ is found in *MrgprA3*- and *MrgprC11*-expressing

neurons, we used *MrgprA3-GFPCre^{tdTomato/+}* mice (8), in which *MrgprA3*⁺ neurons, which include both *MrgprA3* and *MrgprC11* receptors, are labeled with tdTomato fluorescent protein. During patch-clamp recordings, we were able to identify $\text{Na}_v1.9$ currents in all tdTomato⁺ DRG neurons (Figure 3, A and B). Next, we sought to determine coexpression of $\text{Na}_v1.9$ with *MrgprC11* using a validated antibody (54). In this case, we found that 76% of *MrgprC11*⁺ neurons also expressed $\text{Na}_v1.9$ (Figure 3C). Channel expression was rarely observed in substance P⁺ cells (10%), another subset of neurons that have been implicated in coding for itch sensation (refs. 10, 55, and Figure 3D). Although we found $\text{Na}_v1.9$ in a majority of pruriceptors thought to code for itch via members of the *Mrgpr* family, we did not see this Na_v channel subtype in all putative itch neurons.

Loss of $\text{Na}_v1.9$ leads to a reduction in itch. To examine the extent of $\text{Na}_v1.9$ participation in itch, we carried out behavioral tests with our homozygous FAST mice, which contain a Neo-STOP

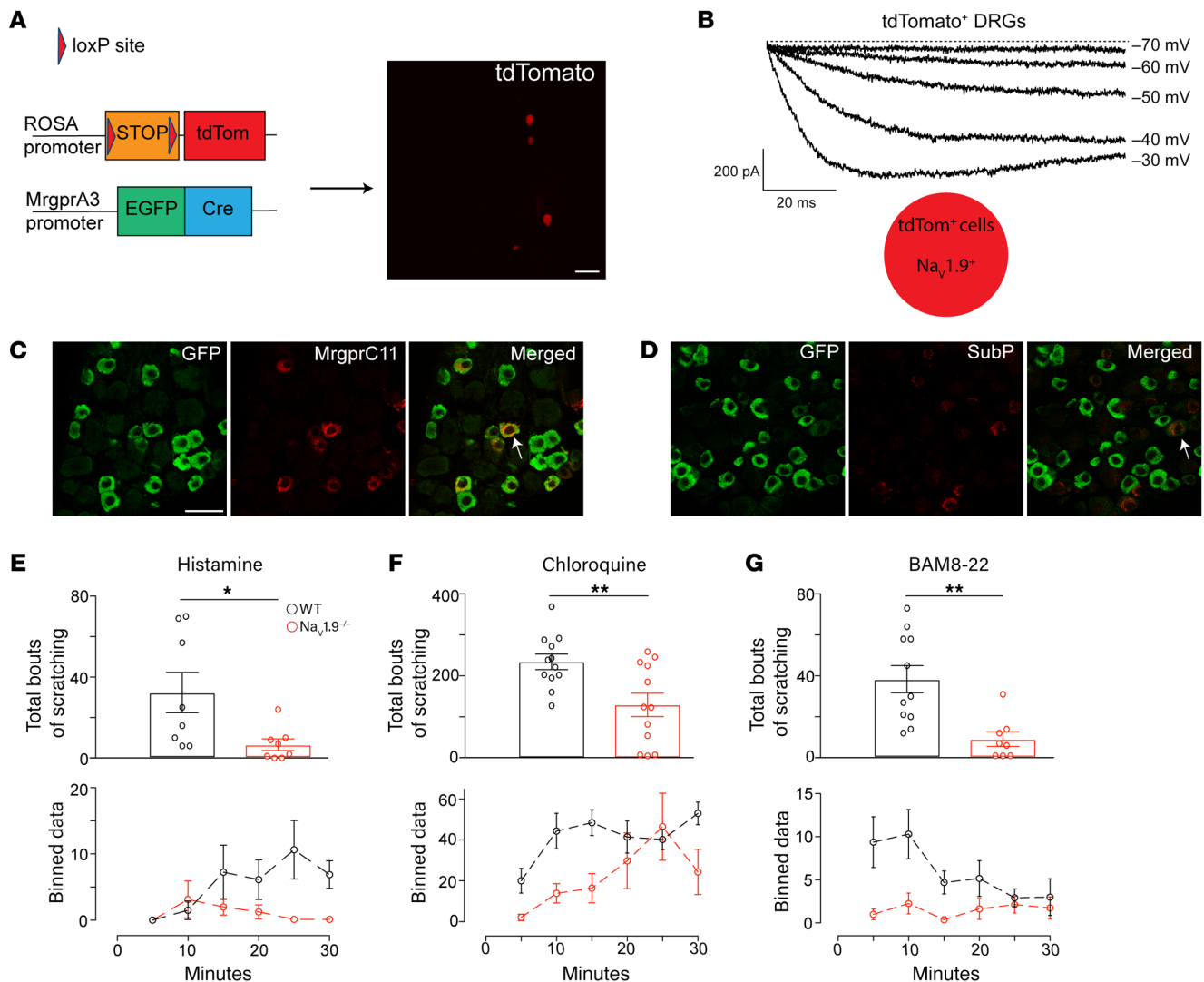


Figure 3. Na_v1.9 expression in MrgprA3⁺ and MrgprC11⁺ neurons and behavioral models. (A) Schematic diagram of the breeding strategy for the MrgprA3-EGFP-Cre^{tdTomato/+} mice showing tdTomato signal (fluorescence was visualized directly without staining). (B) Trace showing Na_v1.9 currents evoked in tdTomato⁺ neurons at the specified voltages. (C) DRG section showing the overlap between neurons stained for GFP and MrgprC11. (D) DRG section illustrating the overlap between neurons stained for GFP and substance P. (E–G) Itch assays with the indicated compound injected into the nape of the neck, recorded for 30-minute intervals, performed in Na_v1.9^{-/-} mice and littermate controls for histamine (E; 8 mice per genotype, $P = 0.02$), CQ (F; 12 mice per genotype, $P = 0.006$), and BAM8-22 (G; WT $n = 11$, Na_v1.9^{-/-} $n = 8$, $P = 0.002$). Panels located directly below each graph (E–G) are the data binned and graphed for every 5 minutes of the recording. * $P < 0.05$, ** $P < 0.01$, by 2-tailed, unpaired Student's t test. Data are represented as mean \pm SEM. Scale bars: 50 μ m.

cassette to generate a global Na_v1.9 knockout line (Na_v1.9^{-/-}), and we compared these results to those with WT littermate controls. We assessed scratching behavior in the FAST mice by subcutaneously injecting pruritic compounds into the nape. The number of bouts of hind paw scratching directed toward the injection site was tallied and binned every 5 minutes. Notably, our Na_v1.9^{-/-} FAST mice exhibited a strong reduction in acute scratching behavior upon histamine application (Figure 3E). Moreover, injection of CQ (MrgprA3 activator) and BAM8-22 (MrgprC11 activator) into these mice also led to a robust decrease in bouts of scratching in comparison with WT littermates, thereby supporting a key role for Na_v1.9 in both histamine-dependent and histamine-independent itch (Figure 3, F and G). It should be noted that although there was no strong response throughout the 30 minutes of recording to

either histamine or BAM8-22 in the Na_v1.9^{-/-} mice (Figure 3, E and G), there appeared to be residual scratching that was delayed in response to CQ in the Na_v1.9^{-/-} mice compared with the littermate WT controls (Figure 3F). This residual scratching behavior could occur due to off-target effects of CQ. Indeed, Liu et al. (9) reported that CQ can also activate mast cells, which may cause an itch behavioral response that is independent of direct MrgprA3 activation. Overall, our results support the importance of Na_v1.9 in both histamine-dependent and histamine-independent itch.

Na_v1.9 is important for histamine- and CQ-evoked Ca²⁺ responses. Histamine, CQ, and BAM8-22 are known to signal via GPCRs, with subsequent activation of TRP channels and increases in internal Ca²⁺ concentrations. Therefore, we wanted to determine whether Ca²⁺ responses were altered after loss of Na_v1.9. We compared Ca²⁺

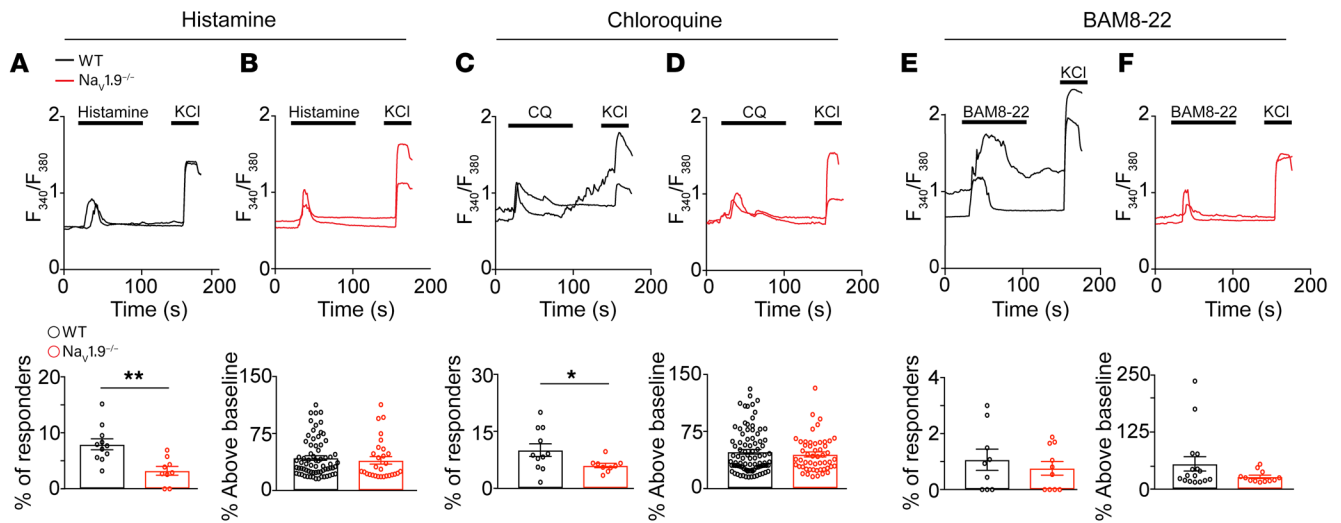


Figure 4. Loss of $\text{Na}_v1.9$ leads to a reduction in histamine- and CQ-responsive but not BAM8-22-responsive neurons. Fura-2 ratiometric Ca^{2+} imaging studies were performed in $\text{Na}_v1.9^{-/-}$ mice and littermate controls. The total percentage of responsive neurons and the magnitude of the Ca^{2+} response were quantified, and representative traces for the Ca^{2+} response after application of each compound are shown. For histamine, the total percentage of responsive neurons was reduced (A; WT and $\text{Na}_v1.9^{-/-}$ $n \geq 800$ cells, $P = 0.0014$), but the magnitude of the response was the same in WT and $\text{Na}_v1.9^{-/-}$ neurons (B; WT and $\text{Na}_v1.9^{-/-}$ $n \geq 800$ cells, $P = 0.59$). For CQ, the percentage of responsive cells was also reduced (C; WT and $\text{Na}_v1.9^{-/-}$ $n \geq 800$ cells, $P = 0.038$), but the magnitude of the response was similar in WT and $\text{Na}_v1.9^{-/-}$ DRGs (D; WT and $\text{Na}_v1.9^{-/-}$ $n \geq 800$ cells, $P = 0.44$). For BAM8-22, no differences were observed for either the percentage of responsive cells (E; WT and $\text{Na}_v1.9^{-/-}$ $n \geq 800$ cells, $P = 0.51$) or the magnitude of the response (F; WT and $\text{Na}_v1.9^{-/-}$ $n \geq 800$ cells, $P = 0.099$). * $P < 0.05$, ** $P < 0.01$, by 2-tailed, unpaired Student's t test for all data represented as mean \pm SEM.

signals after the application of pruritogens in isolated DRGs from $\text{Na}_v1.9^{-/-}$ and WT littermate controls using Fura-2 Ca^{2+} imaging. After the application of histamine (100 μM), we observed that the peak responses in $\text{Na}_v1.9^{-/-}$ mouse DRGs were like those in WT controls (WT, 42.8 ± 3.0 ; $\text{Na}_v1.9^{-/-}$, 39.8 ± 5.0 ; $P = 0.59$) (Figure 4, A and B). However, we found a significant reduction in the total number of neurons that responded to histamine in $\text{Na}_v1.9^{-/-}$ mice compared with WT (WT, $8.0\% \pm 0.8\%$; $\text{Na}_v1.9^{-/-}$, $3.2\% \pm 0.6\%$; $P = 0.0014$) (Figure 4, A and B). Similar effects were seen with CQ (1 mM), with a comparable peak magnitude after the application of CQ in $\text{Na}_v1.9^{-/-}$ and WT DRGs (WT, 48.2 ± 3.1 ; $\text{Na}_v1.9^{-/-}$, 44.8 ± 3.2 ; $P = 0.44$); however, there were significantly fewer responsive neurons (WT, $10.1\% \pm 1.6\%$; $\text{Na}_v1.9^{-/-}$, $6.0\% \pm 0.6\%$; $P = 0.04$) (Figure 4, C and D). Although we did see a similar trend after BAM8-22 application, there were no significant differences, with cells from WT and $\text{Na}_v1.9^{-/-}$ mice showing a comparable magnitude in response to BAM8-22 (WT, 55.2 ± 15.8 ; $\text{Na}_v1.9^{-/-}$, 26.9 ± 3.7 ; $P = 0.09$) and a similar percentage of neurons responding after compound application (WT, $1.1\% \pm 0.4\%$; $\text{Na}_v1.9^{-/-}$, $0.8\% \pm 0.2\%$; $P = 0.5$) (Figure 4, E and F). These observations highlight the importance of $\text{Na}_v1.9$ in Ca^{2+} signaling in both histamine- and CQ-responsive neurons.

Pruritogens influence $\text{Na}_v1.9$ currents. Next, we evaluated the overall electrophysiological properties of WT and $\text{Na}_v1.9^{-/-}$ DRGs identified by Ca^{2+} imaging (Fluo-4) following a brief CQ application and washout. Under these conditions, $\text{Na}_v1.9^{-/-}$ DRGs exhibited a depolarized shift in the resting membrane potential (RMP) of 8.4 ± 3.0 mV ($P = 0.009$) (Figure 5A). AP amplitudes and the threshold to elicit APs (-13.1 ± 1.8 mV in WT and -7.4 ± 3.5 mV in $\text{Na}_v1.9^{-/-}$ neurons; $P = 0.67$) (Figure 5B) were not significantly affected (Table 1). AP kinetics were affected as determined by a higher time to reach the maximum peak (T to peak) of 0.5 ± 0.2

milliseconds ($P = 0.016$) and a lower time to reach the minimum value in the repolarization phase (T to min) of 3.6 ± 1.2 milliseconds ($P = 0.004$) (Table 1). These results are largely in line with previous reports in which AP kinetics were assessed in heterogeneous DRG populations of $\text{Na}_v1.9^{-/-}$ mice (22, 25). In the presence of CQ (100 μM), WT DRGs showed a lower amplitude of 10.4 ± 2.7 mV ($P = 0.002$) and a higher AP threshold of 4.4 ± 2.4 mV ($P = 0.033$), whereas the T to peak and T to min were not affected (Figure 5C and Table 1). Notably, $\text{Na}_v1.9^{-/-}$ DRGs were not affected by the addition of CQ in all parameters tested (Figure 5D), suggesting a key role for $\text{Na}_v1.9$ in CQ-mediated signaling.

Proinflammatory mediators such as PGE_2 , bradykinin, histamine, and ATP can potentiate $\text{Na}_v1.9$ currents (39), which is consistent with the role of $\text{Na}_v1.9$ in inflammatory-induced thermal and mechanical hyperalgesia. Therefore, we determined whether application of either histamine or MrgprA3/MrgprC11 agonist (CQ/BAM8-22) would also lead to increases in DRG TTX-resistant (TTX-R) current density or changes in activation voltage. Since MrgprC11⁺ neurons are a subset of the MrgprA3⁺ population, we used MrgprA3-GFPCre^{tdTomato/+} mice to isolate DRG neurons expressing the receptors for CQ and BAM8-22. We performed patch-clamp experiments in the presence of TTX (300 nM), which blocks all Na_v channel subtypes except $\text{Na}_v1.8$ and $\text{Na}_v1.9$. Additionally, it is established that fluoride ions (F^-) in the pipette permits the partial separation of both Na^+ currents, with $\text{Na}_v1.9$ showing augmented currents and more hyperpolarized activation whereas $\text{Na}_v1.8$ is unaffected (56). Following CQ application, we observed a larger current density at voltage ranges at which only $\text{Na}_v1.9$ is active (Figure 6, A and B, and Table 2). Furthermore, we noted a 15-mV hyperpolarizing shift in channel activation voltage of the TTX-R Na^+ current (Figure 6C). Although we saw sig-

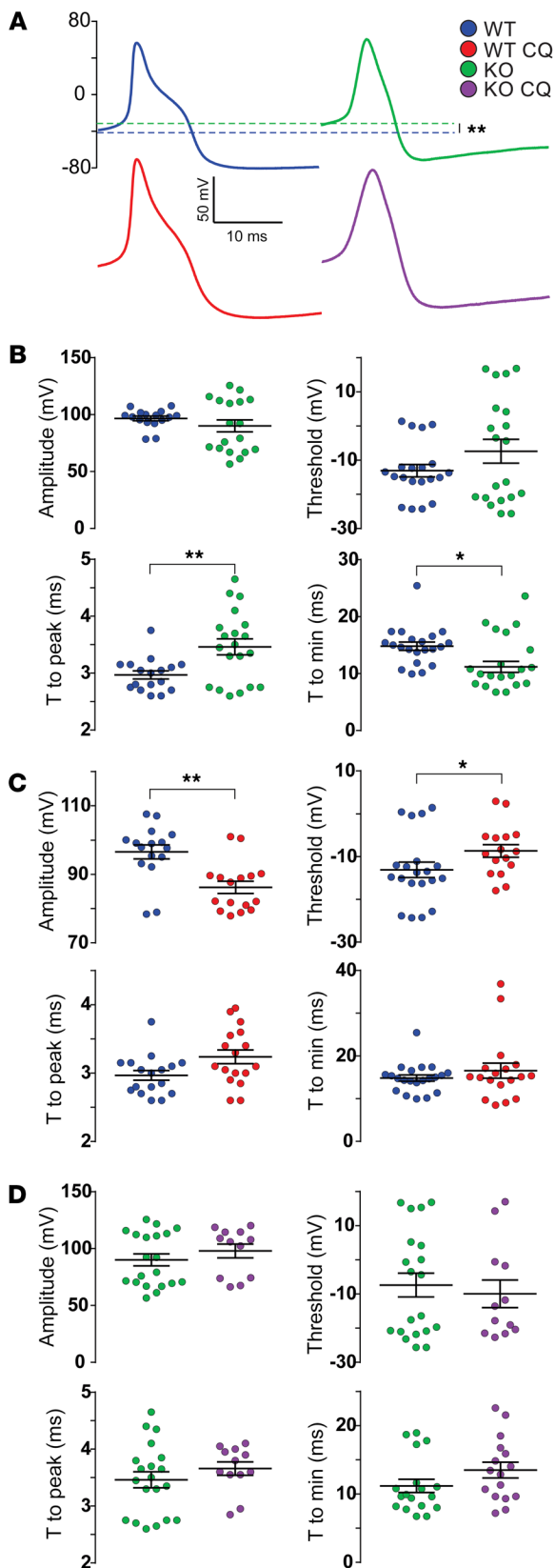


Figure 5. APs are influenced by $Na_v1.9$ and CQ. (A) Representative APs for WT (blue), $Na_v1.9^{-/-}$ (green), WT in the presence of CQ (100 μ M, red), and $Na_v1.9^{-/-}$ mice in the presence of CQ (100 μ M, purple). Dotted lines represent the resting membrane potential (RMP) for WT and $Na_v1.9^{-/-}$: -40.0 ± 1.3 mV and -31.5 ± 2.7 mV, respectively ($n = 13$ for WT and $n = 12$ for $Na_v1.9^{-/-}$; $**P = 0.009$). (B) Quantification of AP parameters in WT and $Na_v1.9^{-/-}$ DRGs. Amplitude of AP (WT $n = 16$ and $Na_v1.9^{-/-}$ $n = 20$, $P = 0.44$) and threshold to elicit an AP were not affected (WT $n = 20$ and $Na_v1.9^{-/-}$ $n = 20$, $P = 0.67$). $Na_v1.9^{-/-}$ APs had a slower time to peak (T to peak; WT $n = 17$ and $Na_v1.9^{-/-}$ $n = 20$, $P = 0.016$) and a faster time to minimum (T to min; WT $n = 21$ and $Na_v1.9^{-/-}$ $n = 18$, $P = 0.004$). (C) CQ treatment affects the AP amplitude and threshold but not kinetics. Amplitude of AP (WT $n = 16$ and with CQ $n = 16$, $P = 0.002$) and threshold to elicit an AP (WT $n = 20$ and with CQ $n = 16$, $P = 0.033$) were significantly lower. T to peak (WT $n = 17$ and with CQ $n = 17$, $P = 0.063$) and T to min (WT $n = 21$ and with CQ $n = 18$, $P = 0.732$) were not significantly different. (D) These effects do not occur in $Na_v1.9^{-/-}$ DRGs: AP ($Na_v1.9^{-/-}$ $n = 20$ and with CQ $n = 12$, $P = 0.5$), the threshold to elicit an AP ($Na_v1.9^{-/-}$ $n = 20$ and with CQ $n = 12$, $P = 0.855$), T to peak ($Na_v1.9^{-/-}$ $n = 20$ and with CQ $n = 12$, $P = 0.219$), and T to min ($Na_v1.9^{-/-}$ $n = 18$ and with CQ $n = 16$, $P = 0.157$) were not statistically significant. $*P < 0.05$, $**P < 0.01$, by 2-tailed, unpaired Student's t test was used for RMP, and Mann-Whitney was used for all other data comparisons, which are represented as mean \pm SEM. See Table 1 for values.

a similar potentiation in $Na_v1.9$ current density at more hyperpolarized potentials (Figure 6, G, H, and J), but no significant differences in $Na_v1.8$ current density (Figure 6, H, K, and L, and Table 2). The application of BAM8-22 also led to an 11.5-mV hyperpolarized shift in activation voltage of the TTX-R current (Figure 6I). Finally, CQ and BAM8-22 accelerated $Na_v1.9$ activation but not $Na_v1.8$ activation (Supplemental Figure 3).

Extensive overlap between CQ- and histamine-responsive neurons has been reported (9). So, we explored whether histamine application (100 μ M) affected TTX-R currents in MrgprA3⁺ (tdTomato⁺) neurons. Although we occasionally saw larger $Na_v1.9$ current densities, we did not find significant potentiation of $Na_v1.9$ or $Na_v1.8$. However, histamine application did result in a 6.5-mV hyperpolarized shift of activation voltage in the TTX-R current (Figure 6, M-R). The observation that not all cells showed this effect in response to histamine can be explained by the population of histamine-responsive neurons only partially overlapping with CQ- and BAM8-22-responsive cells. Therefore, it is possible that the nonresponsive cells lacked the appropriate receptors for histamine.

To further assess whether CQ or BAM8-22 influenced $Na_v1.8$ currents, we transiently transfected mouse $Na_v1.8$ along with MrgprA3 or MrgprC11 in ND7/23 cells. In cells containing $Na_v1.8$ and MrgprA3, we did not see altered channel activation kinetics after the application of CQ; however, we did observe a similar reduction in current densities at a range of voltages (Supplemental Figure 4, A and C). In cells transfected with $Na_v1.8$ and MrgprC11, we noted comparable current densities and channel activation properties before and after application of BAM8-22 (Supplemental Figure 4, B and D).

The $Na_v1.9^{L799P/WT}$ mutation leads to gain of itch in mice. We next used a CRISPR/Cas9 strategy to introduce an orthologous p.L811P (c.2432T>C) gain-of-function mutation into mouse $Na_v1.9$ (L799P/WT; c.2396T>C) against our tetO cassette background (mouse and human $Na_v1.9$ proteins are 73% identical). After 5 backcrossings (first with the B6.C-Tg^(CMV-cre)1Cgn global Cre mouse from The Jackson Laboratory), we performed itch assays on the

nificantly larger $Na_v1.9$ current density (Figure 6D), we observed reduced Na^+ current densities at more depolarized voltages at which Na^+ current is mainly driven by $Na_v1.8$ (Figure 6, E and F, and Table 2). With the application of BAM8-22 (10 μ M), we noted

Table 1. AP parameters of WT and Na_v1.9^{L799P}/MrgprA3⁺ neurons before and after CQ application

	Amplitude of AP (mV)	AP threshold (mV)	APT to peak (ms)	APT to minimum (ms)
WT	96.6 ± 2.1	(-13.1) ± 1.8	3.0 ± 0.1	14.8 ± 0.7
WT after CQ	86.2 ± 1.8 ^B	(-8.7) ± 1.5 ^A	3.2 ± 0.1	16.5 ± 1.8
Na _v 1.9 ^{L799P}	90.1 ± 5.2	(-7.4) ± 3.5	3.5 ± 0.1 ^A	11.2 ± 1.0 ^B
Na _v 1.9 ^{L799P} after CQ	98.0 ± 6.1	(-9.9) ± 4.1	3.7 ± 0.1	13.5 ± 1.2

^A*P* < 0.05 and ^B*P* < 0.01, by Mann-Whitney *U* test for all data comparisons, which are presented as the mean ± SEM.

L799P/WT mouse line and compared the data with those obtained with WT Na_v1.9 mice (Figure 7A). As is the case with human p.L811P^{+/WT} patients, the L799P/WT mice exhibited robust spontaneous scratching when compared with their WT littermate controls (Figure 7B). In virtual agreement with previous observations (22), RT-qPCR analysis of DRGs from sfGFP-Na_v1.9^{L799P/WT} mice revealed a 68% reduction in overall *SCN11a* RNA levels compared with levels in WT controls (Supplemental Figure 5).

Leipold et al. (22) reported a significantly depolarized RMP in DRGs from Na_v1.9^{L799P/WT} mice, which in turn could lead to nerve conduction block as other Na_v channel subtypes expressed in the DRG would inactivate. However, it is possible that some histamine- and/or MrgprA3-positive DRG neurons are hyperexcitable at depolarized RMPs and continue to signal itch stimuli. To test this hypothesis, we first measured Ca²⁺ responses in DRGs from Na_v1.9^{L799P/WT} mice and WT littermate controls in response to histamine, CQ, and BAM8-22. We observed no difference in the number of cells or in the magnitude of the Ca²⁺ response after the application of either histamine or BAM8-22 (Figure 7, C–F). Although we did not observe a difference in the peak response after the application of CQ, we noticed that the percentage of responsive neurons was higher in cells from Na_v1.9^{L799P/WT} mice compared with WT (Figure 4, C and D, and Figure 7, G and H). The depolarized RMP caused by the mutation would reduce the driving force for Ca²⁺ entry via MrgprA3 activation. Since nearly all MrgprA3⁺ neurons express Na_v1.9, it is not unreasonable to assume that the depolarized RMP in Na_v1.9^{L799P/WT} mice (22) pushes the weakly responding CQ neurons to respond more strongly.

Next, we crossed MrgprA3-EGFP^{Cre}^{tdTomato/WT} mice with Na_v1.9^{L799P/WT} mice to investigate the excitability of MrgprA3⁺ neurons. The resulting mouse line allowed us to perform current-clamp experiments on MrgprA3⁺ DRGs expressing the mutant channel. Similar to what was reported before (22), we found a significantly depolarized RMP in MrgprA3⁺ neurons from Na_v1.9^{L799P/WT} mice compared with littermate controls (WT, -40.0 ± 1.3 mV; mutant, -23.9 ± 1.8 mV; *P* = 0.0007, *n* = 21) (Figure 7I). Most tested MrgprA3⁺ neurons containing the mutant channel were unable to generate APs, even in response to large current injections (17 of 21 cells; Figure 7K). However, a small DRG subset (4 of 21 cells) was able to fire at a depolarized RMP, even in response to current injections as low as 10 pA, and repetitive APs at 50 pA, which was substantially less than the current needed to evoke APs for WT MrgprA3⁺ neurons (>50 pA; Figure 7, J and L).

Discussion

While the symptom of itch is prevalent and has a substantial disease burden, it remains challenging to address. Thus, new ther-

apeutics for pathological itch are needed. While Na_v1.9 has a proven role in pain (31), the role of this Na_v channel subtype in itch is less understood. Here, we report a clinical case of a patient with a heterozygous Na_v1.9 p.L811P mutation who suffers from unbearable pruritis (Figure 1A). To better understand Na_v1.9 involve-

ment in itch, we developed an N-terminally sfGFP-tagged Na_v1.9 mouse line. Using this mouse line, we determined that this channel subtype was expressed primarily in a subset of nonmyelinated, nonpeptidergic small-diameter DRGs that typically contain MrgprA3 or MrgprC11 (Figure 1B, Figures 2 and 3, and Supplemental Figures 1 and 2).

Our studies revealed a strong reduction in acute scratching behavior in Na_v1.9^{L799P} animals with itch evoked by administration of histamine, CQ, or BAM8-22 compared with WT controls (Figure 4). Moreover, several AP parameters in WT DRGs were altered by CQ but not in the absence of Na_v1.9 (Figure 5). It is noteworthy that Na_v1.9^{L799P} mice still scratched moderately in response to administration of CQ, a possible off-target effect of this compound. Indeed, Liu et al. measured CQ-induced scratching bouts in SASH mice, which lack mast cells, and still found a significant reduction in the total bouts of scratching in comparison with controls (9).

While it is challenging to extrapolate the obtained results to humans (22, 28, 30), Na_v1.9^{L799P/WT} mice displayed an increased frequency of spontaneous scratching, as is the case with human patients (Figure 7). Previous work has shown that this mutation can lead to a slowing of deactivation as well as a hyperpolarizing shift in channel availability, which in turn would lead to excess Na⁺ influx that can subsequently inactivate other Na_v channel subtypes to cause conduction block (22). Indeed, we found that most MrgprA3⁺ neurons from Na_v1.9^{L799P/WT} mice were unable to fire APs even in response to large current injections. However, a subset of MrgprA3⁺ neurons with depolarized RMPs could still fire APs in response to current injections as small as 10 pA, much less than for most WT MrgprA3⁺ neurons (Figure 7, I–L). Therefore, it is possible that this small subset of hyperexcitable MrgprA3⁺ neurons (~20%) may contribute to the increase in spontaneous itch seen in the Na_v1.9^{L799P/WT} mice and in human patients. Although other Na_v channel subtypes, such as Na_v1.7 (57) and Na_v1.8 (19), may also be involved in transmitting pruritic stimuli, it is striking that loss of Na_v1.9 leads to such drastic reductions in acute itch (Figure 3). All 3 pruritic compounds potentiate Na_v1.9 currents in mouse DRGs without affecting Na_v1.8, except CQ, which influences both Na_v1.8 and Na_v1.9 currents (Figure 6 and Supplemental Figures 3 and 4). However, BAM8-22 activity predominantly affects Na_v1.9 activation. Furthermore, CQ and BAM8-22 speed up the kinetics of activation of Na_v1.9, making it more likely to contribute to the upstroke of the AP. Finally, activation of MrgprA3⁺ neurons with either of these compounds leads to significant hyperpolarized activation of TTX-R currents. Thus, it is conceivable that Na_v1.9 inhibitors administered to p.L811P patients can decrease itch while restoring, at least in part, pain sensations (22, 28). To identify such

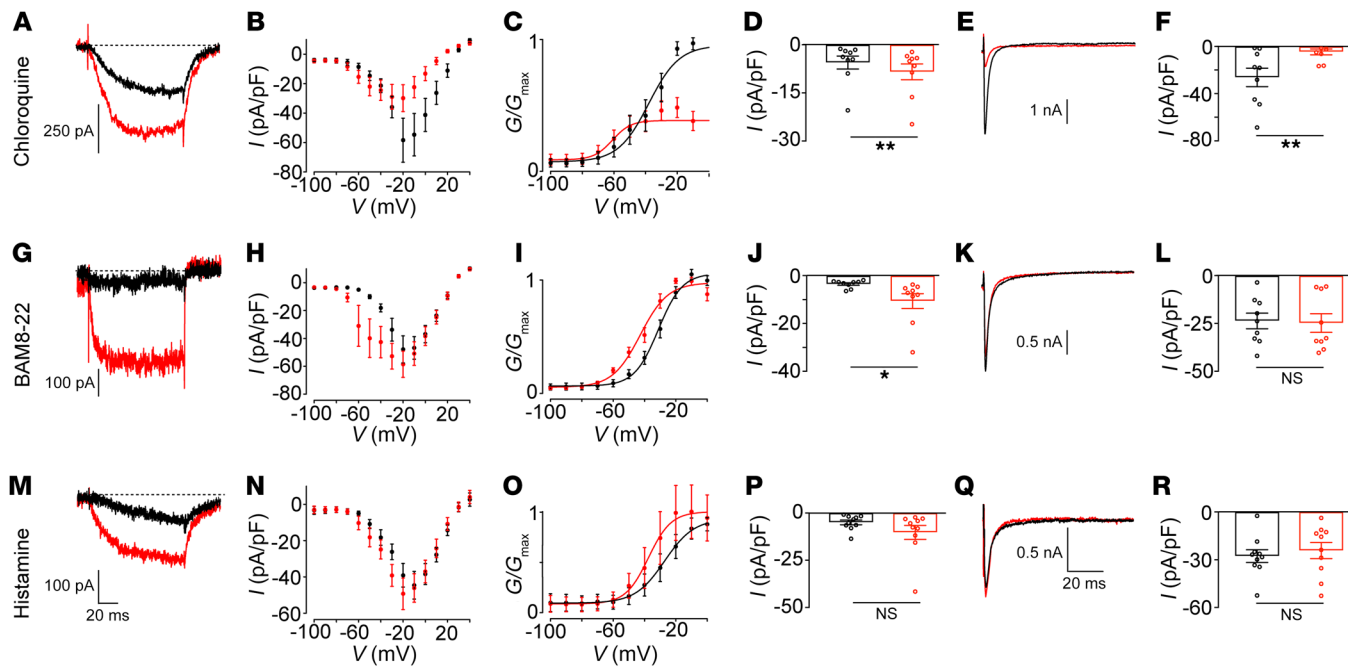


Figure 6. Application of CQ, BAM8-22, and histamine leads to a potentiation of $\text{Na}_v1.9$ current and a shift in activation voltage of TTX-R current.

Voltage-clamp recordings from $\text{MrprA3-Cre}^{\text{tdTomato/+}}$ DRGs. (A) Sample current trace at -70 mV shows that CQ application potentiates $\text{Na}_v1.9$ current. (B) Current-voltage (I - V) relationship of the TTX-resistant (TTX-R) current before and after CQ application. (C) Conductance-voltage (G - V) plot for TTX-R current shows a 15.7 -mV hyperpolarized shift in activation voltage ($n = 9$, $P = 0.002$). (D) $\text{Na}_v1.9$ current density (pA/pF) is higher after CQ ($n = 9$, $P = 0.004$). (E and F) Sample trace of $\text{Na}_v1.8$ shows a decrease of current density after CQ administration ($n = 9$, $P = 0.005$). (G) Current trace at -70 mV shows a larger $\text{Na}_v1.9$ current density after BAM8-22. (H) I - V for TTX-R current before and after BAM8-22. (I) G - V for TTX-R current shows an 11.5 -mV hyperpolarized shift in activation after BAM8-22 application ($n = 9$, $P = 0.012$). (J) $\text{Na}_v1.9$ current density is higher after BAM8-22 ($n = 9$, $P = 0.049$). (K and L) $\text{Na}_v1.8$ current and current density shows no differences before and after administration of BAM8-22 ($n = 9$, $P = 0.68$). (M) Current trace at -60 mV shows a moderate $\text{Na}_v1.9$ potentiation after histamine administration. (N) I - V for TTX-R before and after histamine administration. (O) G - V for TTX-R current after histamine shows a 6.5 -mV hyperpolarized shift in activation voltage ($n = 10$, $n = 0.029$). (P) $\text{Na}_v1.9$ current density shows no significant change after histamine addition ($n = 10$, $P = 0.14$). (Q and R) $\text{Na}_v1.8$ current and current density shows no differences before and after histamine application ($n = 9$, $P = 0.41$). $\text{Na}_v1.9$ and $\text{Na}_v1.8$ currents before (black) and after (red) compound application are shown. * $P < 0.05$, ** $P < 0.01$. A 2-tailed, unpaired and paired Student's t test was used for all analyses. Data represent the mean \pm SEM. See Table 2 for values.

compounds, a dependable $\text{Na}_v1.9$ cell line is of great value in drug screening experiments. Therefore, we developed such a tool using intron-mediated enhancement of gene expression, an approach that may also be useful to enhance heterologous expression of other ion channels (Figure 1, F and G). The peripherally restricted expression of $\text{Na}_v1.9$ should be beneficial in limiting adverse side effects of therapeutics. Altogether, the insights reported here can help us better understand itch, and show that $\text{Na}_v1.9$ constitutes an attractive pharmacological target to relieve pathological itch.

Methods

Case report and subject details. Written authorization for the release of health information in the case report was obtained from the patient's parent (her legal guardian) in accordance with the guidelines of the Johns Hopkins Medicine Institutional Review Board. The patient verbally assented, the parent supplied the photograph used in this publication, and the parent and patient approved the written content of the paragraph describing her clinical features and the layout of the picture showing the scars. All personal information that could lead to identification has been removed.

Mouse lines. FAST $\text{Na}_v1.9$ mice were generated by Ingenious Targeting Laboratory (iTTL) technologies. $\text{Na}_v1.8$ -Cre mice were provided

by Michael Caterina (Johns Hopkins University School of Medicine, Baltimore, Maryland, USA). Ai9(RCL-tdTomato) mice were acquired from The Jackson Laboratory. All experiments were performed using protocols approved by the Animal Care and Use Committee of Johns Hopkins University School of Medicine. Two- to four-month-old male and female mice were backcrossed to C57BL/6J in our mouse colony for at least 5 generations. We housed 4–5 mice in each cage in the vivarium with a 12-hour light/12-hour dark cycle and an ad libitum food and water supply.

Behavioral itch assays. All mouse behavior tests were performed and analyzed with the experimenter blinded to genotype. Male and female mice (8–12 weeks old, 20–30 g each) were used for experimentation. All itch behavior was performed between 8 am and 12 pm. On the day before the experiment, animals were placed in the test chamber for 30 minutes before undergoing a series of 3 mock injections with 5-minute breaks in between. On the day of the experiment, animals were allowed to acclimatize to the test chamber for 10 minutes before injection. Pruritic compounds were injected s.c. into the nape, and scratching behavior was observed for 30 minutes. A bout of scratching was defined as a continuous scratching, not wiping, movement by either hind paw directed at the area of the injection site. Scratching behavior was quantified by counting of the number of scratching bouts

Table 2. Influence of pruritogens on the biophysical characteristics of TTX-R currents in MrgprA3⁺ DRGs

	V _{1/2} activation (mV)	Current density (pA/pF)
TTX-R before CQ	(-38.4) ± 4.8	
TTX-R after CQ	(-54.2) ± 3.9 ^B	
Na _v 1.9 before CQ		(-5.6) ± 2.0
Na _v 1.9 after CQ		(-8.1) ± 2.5 ^B
Na _v 1.8 before CQ		(-26.3) ± 7.8
Na _v 1.8 after CQ		(-4.6) ± 2.5 ^B
TTX-R before BAM8-22	(-32.0) ± 2.2	
TTX-R after BAM8-22	(-43.5) ± 1.9 ^A	
Na _v 1.9 before BAM8-22		(-3.5) ± 0.6
Na _v 1.9 after BAM8-22		(-10.6) ± 3.3 ^A
Na _v 1.8 before BAM8-22		(-23.7) ± 4.1
Na _v 1.8 after BAM8-22		(-24.8) ± 4.9
TTX-R before histamine	(-28.5) ± 4.8	
TTX-R after histamine	(-35.0) ± 4.2 ^A	
Na _v 1.9 before histamine		(-5.0) ± 1.2
Na _v 1.9 after histamine		(-10.3) ± 3.7
Na _v 1.8 before histamine		(-27.8) ± 3.9
Na _v 1.8 after histamine		(-24.3) ± 5.0

^AP < 0.05 and ^BP < 0.01, by 2-tailed, unpaired and paired Student's *t* test for all analyses. Data are presented as the mean ± SEM.

over the 30-minute observation period. Concentrations used for all compounds were 1 mM dissolved in physiological saline.

Cultures of dissociated DRG neurons. Adult mice (8–12 weeks old) were anesthetized with CO₂ followed by cervical dislocation. The spinal column was removed and trimmed of excess muscle. The vertebral column was then bisected, and one side was placed into a Petri dish with cold bicarbonate-free DMEM (bfDMEM; Thermo Fisher Scientific), while the DRGs were collected from the other side. In a separate Petri dish, DRGs were collected into cold bfDMEM. Once all ganglia were collected, forceps and fine scissors were used to trim excess nerve roots from the ganglia. Trimmed ganglia were placed into a 15-ml Falcon tube with 4 ml of enzyme mix for 30 minutes at 37°C. The enzyme mix consisted of 0.78 mg/ml of protease (Worthington) and 1.25 mg/ml collagenase I (Worthington) in 4 ml of bfDMEM. After incubation, the ganglia were centrifuged at 50 rpm for 5 minutes. The enzyme solution was removed, and ganglia were washed with complete DMEM (10% FBS, 1× penicillin/streptomycin) and then centrifuged at 600 rpm. After the centrifugation step, ganglia were triturated with 1-ml pipette tips 20–30 times or until no large chunks of tissue remained. The dissociated cells were put through a 100-µm strainer (Thermo Fisher Scientific). The cells were then centrifuged for 5 minutes at 600 rpm. After this step, the overlying solution was removed and replaced with 200–400 µl or a volume of cell culture medium (complete DMEM, 10% FBS, 1× penicillin/streptomycin) necessary to drop the desired density of cells onto poly-D-lysine-coated coverslips in 24-well plates (Thermo Fisher Scientific). About 60–80 µl of cell solution was applied to the center of the coverslip. Cells were allowed

to settle for 30 minutes, and then the well was flooded with 500 µl of additional cell culture medium.

Immunofluorescence. Adult mice (8–12 weeks old) were anesthetized with CO₂ and perfused with 15 ml 0.1 M PBS (pH 7.4, 4°C) followed by 25 ml of fixative (4% paraformaldehyde [vol/vol] and 14% saturated picric acid [vol/vol] in PBS, 4°C). Spinal cord and DRGs were dissected from perfused mice. DRG was postfixed in fixative at 4°C for 30 minutes, and spinal cords were fixed for 2 hours. Skin was dissected from nonperfused mice and fixed in 2% paraformaldehyde (vol/vol) for 2–4 hours at 4°C. After fixation, tissues were washed with 0.1 M PBS 3 times for 5 minutes each. All tissues were cryoprotected in 20% sucrose (wt/vol) for more than 24 hours and were sectioned with a cryostat at 20 µm for DRGs and nerves and 30 µm for spinal cord and skin. DRGs and nerve sections were dried at 37°C for 30 minutes. An antigen retrieval step was also conducted with sodium citrate (10 mM, pH 6, and 0.05% Tween-20) for 10 minutes at 85°C, followed by 3 washes 5 minutes each with 0.1 M PBS. Tissue was preincubated with blocking solution (10% FBS [vol/vol], 0.1% Triton X-100 [vol/vol] in PBS, pH 7.4) for 1–2 hours, and then incubated overnight at 4°C with primary antibodies. Secondary antibody incubation was performed for 2 hours in blocking solution at 22°C–23°C. Three washes with PBS (0.1% Triton X-100) for 5 minutes each were performed in between incubations. For spinal cord and skin, cryostat sections were cut to 30 µm and placed in 0.1 M phosphate buffer for whole-mount immunostaining. Sections were then incubated in blocking solution for 1 hour at room temperature. Next, sections were incubated in primary antibody overnight at 4°C with gentle shaking for at least 24 hours. Primary incubation was followed by 3 washes for 5 minutes each, followed by incubation with secondary antibody for 2 hours at room temperature. Finally, sections were washed 3 more times for 5 minutes each, followed by 2 washes with H₂O, and mounted onto coverslips. The following primary antibodies were used: chicken anti-GFP (1:2,000; GFP-1020, Aves Labs), rabbit anti-sfGFP (1:2,000; gift from Ramanujan Hegde, University of Cambridge, Cambridge, United Kingdom); rabbit anti-GFP (1:2,000; ab290, Abcam); rabbit anti-NF200 (1:500; AB1989, Millipore); rabbit anti-substance P (1:1,000; AB1566, Millipore); rabbit anti-tyrosine hydroxylase (1:500; P40101-150, Pel-Freez); goat anti-c-Ret (1:500; AF482, Novusbio); rabbit anti-PGP9.5 (1:500; PA5-29012, Thermo Fisher Scientific); rabbit anti-CGRP (1:500; T-4239, Peninsula Laboratories); and anti-peripherin (1:200; ab4666, Abcam). To detect IB4 binding, sections were incubated with biotinylated *Griffonia simplicifolia* isolectin GS-IB4 (1:500; B-1205, Vector Laboratories). For secondary antibodies, we used donkey anti-rabbit (A31572, Alexa Fluor 555 conjugated), goat anti-chicken (A21103, Alexa Fluor 488 conjugated), and rabbit anti-goat (A214310, Alexa Fluor 555 conjugated) (all from Thermo Fisher Scientific), and for biotinylated IB4, we used streptavidin (DyLight 549, SA-5549, Vector Laboratories). All secondary antibodies were diluted at 1:500 in blocking solution.

Western blot. Adult mice (8–12 weeks old) were anesthetized with CO₂ followed by cervical dislocation. DRGs and trigeminal ganglia were dissected out and placed in 300 µl lysis buffer (in mM: 320 sucrose; 10 HEPES; 2 EDTA, pH 8.0; 1.25% Triton X-100; 50 U/ml benzonase; Roche Protease Inhibitor Mini Tablet). Tissue was homogenized in a 1-ml Dounce homogenizer for 5–10 minutes on ice. The samples were then allowed to rotate at 4°C for 1 hour. Following this step, tissue solution was centrifuged at 15,000 rpm for 20 minutes at 4°C. The supernatant with protein was removed and placed

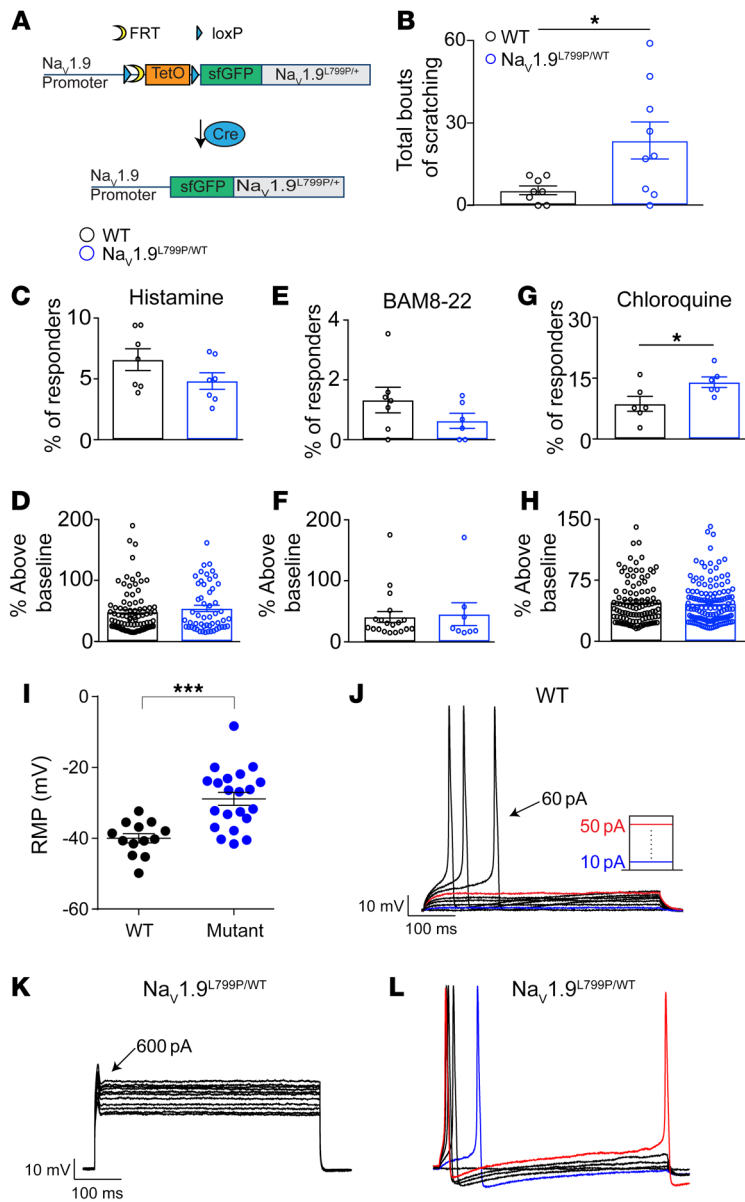


Figure 7. sfGFP- $\text{Na}_v1.9^{\text{L799P/WT}}$ mice show higher basal scratching and more CQ-responsive neurons. (A) Schematic diagram showing the initial cassette inserted to generate sfGFP- $\text{Na}_v1.9^{\text{L799P/WT}}$ mice and subsequent breeding to generate mice for experimentation. (B) sfGFP- $\text{Na}_v1.9^{\text{L799P/WT}}$ mice showed a higher level of scratching compared with their littermate controls (WT $n = 8$, sfGFP- $\text{Na}_v1.9^{\text{L799P/+}}$ $n = 9$, $P = 0.043$). (C–H) Fura-2 ratiometric Ca^{2+} imaging studies were performed in sfGFP- $\text{Na}_v1.9^{\text{L799P/+}}$ mice and littermate controls. No differences were seen after histamine application in either the total percentage of responsive neurons (C; WT and sfGFP- $\text{Na}_v1.9^{\text{L799P/WT}}$ $n \geq 700$ cells, $P = 0.15$) or the magnitude of the response (D; WT and $\text{Na}_v1.9^{\text{L799P/+}}$ $n \geq 700$ cells, $P = 0.36$). For BAM8-22, no differences were observed for either the percentage of responsive cells (E; WT and sfGFP- $\text{Na}_v1.9^{\text{L799P/WT}}$ $n \geq 700$ cells, $P = 0.19$) or the magnitude of the response (F; WT and sfGFP- $\text{Na}_v1.9^{\text{L799P/WT}}$ $n \geq 700$ cells, $P = 0.83$). For CQ, the percentage of responsive cells was significantly higher (G; WT and sfGFP- $\text{Na}_v1.9^{\text{L799P/WT}}$ $n \geq 700$ cells, $n = 0.042$), but no difference was seen in the magnitude of the response (H; WT and sfGFP- $\text{Na}_v1.9^{\text{L799P/WT}}$ $n \geq 700$ cells, $P = 0.59$). (I) RMPs in MrgprA3^+ DRGs from WT (-40.0 ± 1.3 mV, $n = 13$) and $\text{Na}_v1.9^{\text{L799P/WT}}$ (-23.9 ± 1.8 mV, $n = 21$) mice differ significantly ($P = 0.0007$). (J–L) WT MrgprA3^+ neurons require ≥ 50 pA current injection to spike (J), whereas $\text{MrgprA3}^+; \text{Na}_v1.9^{\text{L799P/WT}}$ DRGs consist of a subset (17/21) that does not fire AP at large current injections (≥ 500 pA; RMP = -42 mV) and a smaller group (4/21) that fires in response to current injections as low as 10 pA and repetitive APs at 50 pA (RMP = -26 mV) (K and L). $*P < 0.05$ and $***P < 0.001$, by 2-tailed, unpaired Student's t test for Ca^{2+} imaging/current-clamp experiments and Mann-Whitney test for behavioral comparisons. Data are represented as mean \pm SEM.

into a new tube and stored at -20°C until further use. All other tissue was placed into lysing beads (Matrix D, MP Biomedicals) in 2-ml tubes and kept on ice. The tubes were then placed into a benchtop homogenizer (FastPrep-24 Classic Instrument homogenizer, MP Biomedicals) and homogenized using a custom-made program (speed 4 m/s for 20 seconds). This step was repeated if the tissue was not completely homogenized. The samples were then centrifuged at 15,000 rpm for 20 minutes. Supernatant with protein was removed and placed into a new tube and stored at -20°C until further use. Protein concentration was determined using a BCA assay (Pierce). All protein samples were appropriately diluted in $1\times$ LDS (Thermo Fisher Scientific) plus reducing agent (Thermo Fisher Scientific). Ten micrograms of protein was run on 3%–8% Tris-acetate gels (Thermo Fisher Scientific) with Tris-acetate running buffer and analyzed by Western analysis. Nitrocellulose membranes were incubated in blocking buffer (5% BSA, 0.1% Tween-20, in $1\times$ TBS) and then probed overnight at 4°C with appropriate primary antibodies and 2 hours at room temperature with 1:10,000 goat anti-mouse HRP-conjugated antibody

as secondary antibody (Thermo Fisher Scientific). Membranes were incubated for 5 minutes with an enhanced chemiluminescent substrate before imaging (Thermo Fisher Scientific). Primary antibodies used were rabbit anti-sfGFP (1:2,000; gift from Ramanujan Hegde), rabbit anti- $\text{Na}_v1.9$ (1:5,000; ASC-017, Alomone Labs), and rabbit anti-HSP90 (1:1,000; C45G5, Cell Signaling).

Generation of ND7/23 stable cell lines. ND7/23 FRT cell lines (Sigma-Aldrich) were generated using the Flp-In system (Thermo Fisher Scientific) per protocol instructions. For the generation of sfGFP- $\text{Na}_v1.9$ and $\text{Na}_v1.9$ ND7/23 stable cell lines with intron 2 (synthesized by Genscript), ND7/23 FRT cells were grown to 20% confluence and cotransfected with the pOG44 vector (Thermo Fisher Scientific) and either sfGFP- $\text{Na}_v1.9$ or $\text{Na}_v1.9$ inserted into the pcDNA5/FRT vector (Thermo Fisher Scientific) at a ratio of 9:1, using the Lipofectamine 3000 protocol (Thermo Fisher Scientific) per protocol instructions. Twenty-four hours after transfection, cells were washed and fresh cell culture medium (complete DMEM) was added. Forty-eight hours after transfection, the cells were split onto a fresh 6-well plate so that they

were no more than 25% confluent. After the cells were allowed to settle for 2–3 hours, fresh culture medium with the appropriate amount of hygromycin (150 $\mu\text{g}/\text{ml}$) (Thermo Fisher Scientific) was added. Non-transfected ND7/23 FRT cells were used as a negative control. The cell culture medium was replaced every 2–3 days, and the transfected cells could grow until no cells remained in the control plates. After this, cells were split and allowed to grow for an additional passage, before use for future experiments or freezing. Transient transfections of mouse $\text{Na}_v1.8$ (NM_001205321; Origene Technologies) with either MrgprA3 or MrgprC11 were performed with Lipofectamine 3000 (Thermo Fisher Scientific) per protocol instructions.

Ca²⁺ imaging. DRG neurons from male and female $\text{Na}_v1.9^{-/-}$ and $\text{Na}_v1.9^{\text{L799P/+}}$ mice (8–12 weeks old) and littermate controls were dissociated using an established DRG dissociation protocol (see above) and used for Ca^{2+} imaging studies within 36 hours after dissociation. All recordings and appropriate compound dilutions were done in modified Ringer's solution (in mM: 140 NaCl, 5 KCl, 10 HEPES, 2 MgCl_2 , 2 CaCl_2 , 10 glucose, pH 7.4). Neurons were loaded with Fura-2-acetoxymethyl ester (2.5 mM; Thermo Fisher Scientific) plus 0.02% Pluronic F-127 (Thermo Fisher Scientific) for 1 hour in the dark at 22°C. After washing twice, cells were imaged at 340- and 380-nm excitation to detect intracellular free Ca^{2+} . The protocol for all imaging experiments included a brief wash, followed by 90 seconds of histamine (100 μM ; Sigma-Aldrich), CQ (1 mM; Sigma-Aldrich), or BAM8-22 (10 μM ; Sigma-Aldrich) application, another brief wash, and finally a 30-second application of high KCl (75 mM) to identify neurons. Cells that did not show a response to high KCl were discarded from our analysis. Cells were counted as responding that had a peak 340/380 ratio response 15% above baseline. All experiments were done in triplicate. For each compound, a total of 700–1,000 neurons from 3 mice of the specified genotype were used for analysis. Analysis of the images was performed with the experimenter blind to the genotype.

Electrophysiological recordings of DRGs and ND7/23 cells. Pipettes were fabricated from borosilicate glass (A-M Instruments) and pulled to 1.0–2.5 M Ω using a P-1000 puller (Sutter Instruments). A multi-clamp 700B (Molecular Devices) amplifier with pClamp 10 software (Molecular Devices) was used to acquire data. Series resistance for all cells was corrected electronically up to 70%. All recordings were done at room temperature. Current- and voltage-clamp recordings were obtained using whole-cell configurations in isolated DRGs using the dissociation protocol described above. Linear leak and capacitive transients were subtracted electronically using the $-P/4$ protocol. Data were acquired at 20 kHz and filtered at 2 kHz. Two percent agar bridges filled with bath solution served as the reference electrode.

For voltage-clamp recordings, bath solutions contained (in mM): 3 KCl, 10 glucose, 10 HEPES, 10 tetraethylammonium Cl, 40 NaCl, 90 choline Cl, 2.5 CaCl_2 , 1 MgCl_2 , 0.05 CdCl_2 , pH 7.35, 308 mOsm. Intracellular solutions contained (in mM): 100 CsCl, 30 CsF, 5 NaCl, 2.4 CaCl_2 , 1 MgCl_2 , 5 EDTA (pH 8), 10 HEPES, 4 MgATP, pH 7.3, 303 mOsm. Osmolarity and pH were adjusted with sucrose and NaOH, respectively.

For heterologous expression of $\text{mNa}_v1.8$ (clone obtained from Origene) with either MrgprA3 or GFP-MrgprC11, ND7/23 cells were transfected 2 days before recording with Lipofectamine 3000 (Thermo Fisher Scientific) per protocol instructions. Cells transfected with $\text{mNa}_v1.8$ and MrgprA3 were also cotransfected with mCherry to help identify successfully transfected cells.

For recordings, cells were allowed to equilibrate for 10 minutes before seals were obtained. Recordings were done 10 minutes after whole-cell configuration was obtained to allow dilution of cell interior with the intracellular solution. Peak currents were measured using either 300-ms or 100-ms pulses between -100 mV and $+60$ mV every 10 seconds from a holding potential of -120 mV. The peak current was also normalized to cell capacitance and plotted against the voltage to obtain current density–voltage relationships. The normalized G - V curves were fit with the Boltzmann function: $G = 1/(1 + \exp[(V - V_{1/2}]/k))$, to determine $V_{1/2}$. Time to peak was obtained by measurement of the time from beginning of voltage step to peak current. Activation time constant was obtained via a single-exponential fit (Clampfit 10, Molecular Devices). Other data analysis software used included Microsoft Excel and Origin 8 (Originlabs).

For current-clamp recordings, bath solutions contained (in mM): 150 NaCl, 4 KCl, 2 CaCl_2 , 2 MgCl_2 , 10 glucose, 10 HEPES, pH 7.4 adjusted with NaOH, 310 mOsm. Intracellular solutions contained (in mM): 140 K-gluconate, 13.5 NaCl, 1.6 MgCl_2 , 0.09 EDTA (pH 8), 9 HEPES, 4 MgATP, 14 Tris creatine PO_4 , 0.3 NaGTP, pH 7.4 adjusted with KOH, 311 mOsm. Resting membrane potential was measured in $I = 0$ (zero current mode) for 30 seconds immediately after whole-cell configuration was established. AP thresholds were measured by a series of 100-ms, 10-pA depolarizing current injections. At the minimal current injection needed to elicit an AP, firing threshold was determined by calculation of the potential at which the rate of rise crossed 10 V/s. Amplitude of the AP was determined as the difference between the voltage values at the peak and at the baseline before stimulation. Time to peak corresponded to the time between the threshold and the maximum peak, and time to minimum to the time between the maximum and the minimum value observed in the hyperpolarization phase. Data were analyzed offline with Clampfit 10 and Axograph X (Molecular Devices).

RT-qPCR analysis. DRGs were extracted from 8- to 12-week-old mice. Total RNA was extracted from samples using RNeasy Mini Kit according to the manufacturer's instructions (Qiagen). TURBO DNA-free kit was used to remove contaminating DNA (Invitrogen). Samples were then converted to cDNA using SuperScript III First-Strand Synthesis System for RT-PCR (Invitrogen). TaqMan primers for mouse *SCN11a* and 18S rRNA were designed and ordered from Invitrogen. RT-qPCR reactions consisted of 1 μl of 1:100 cDNA dilution, 5 μl TaqMan PCR Master Mix (Invitrogen), 0.5 μM primers, and up to 10 μl with deionized water. All samples were run in triplicate using Applied Biosystems QuantStudio 6 Flex Real-Time PCR system. The $\Delta\Delta\text{Ct}$ method was used to quantify relative amounts of cDNA for each gene of interest normalized to 18S rRNA.

Quantification and statistical analysis. Data are presented as mean \pm SEM. “ n ” represents the number of samples analyzed. Statistical analysis was performed with 2-tailed Student's t test, Mann-Whitney U test, or 1-/2-way ANOVA as indicated in the figure legends. No data were excluded. Differences were considered statistically significant if P was less than 0.05. Representative data are from experiments that were replicated biologically at least 3 times with similar results. Detailed statistical analyses are mentioned in the figure legends. Statistical analysis was done with GraphPad Prism 7.04 and Microsoft Excel.

Study approval. The Animal Care and Use Committee of Johns Hopkins University School of Medicine approved all mouse experiment protocols.

Author contributions

JS, MDB, JM, XD, and FB designed experiments. ET obtained patient clinical data, wrote the patient report, and meet the current International Committee of Medical Journal Editors criteria for authorship. JS carried out mouse line characterizations, immunostaining, Western blots, electrophysiology, behavioral studies, and calcium imaging. MDB was involved in the electrophysiological characterization of tissues. JM performed behavioral experiments. JS, MDB, and JM analyzed data. JS, MDB, and FB wrote the manuscript, and the other authors approved the manuscript.

Acknowledgments

This work was supported by a Department of Defense National Defense Science and Engineering Graduate Fellowship (to JS), a Blaustein Pain Research grant, a Johns Hopkins Catalyst Award, and a Johns Hopkins Bridge Funding Award to FB; the Hugo W.

Moser Research Institute at Kennedy Krieger Inc. (to ET); a T32 GM007445 training grant; and NIH grants R01DE022750 and R01NS054791 to XD. XD is an Investigator of the Howard Hughes Medical Institute. We thank Peilin Shen for expert help with managing the mouse colonies, C. Hawkins and the staff of the Transgenic Mouse Core at Johns Hopkins University for assistance with transgenic mouse lines, Liang Han for the MrgprC11 antibody, and Roger Reeves, Michael Caterina, Matthias Ringkamp, and the members of the Bosmans laboratory for helpful discussions.

Address correspondence to: Juan Salvatierra, Department of Anatomy, UCSF, 1550 Fourth St., San Francisco, California 94158, USA. Phone: 410.955.4428; Email: jjstierra@gmail.com. Or to: Frank Bosmans, Physiology Group, Ghent University, Corneel Heymanslaan 10, Building B, Entrance 36, 9000 Ghent, Belgium. Phone: 410.955.1609; Email: frankbosmans@outlook.com.

- Kandel ER, Schwartz JH, Jessell TM, Siegelbaum SA, Hudspeth AJ. *Principles of Neural Science*. 5th ed. New York, New York, USA: McGraw-Hill Medical; 2012.
- Green D, Dong X. The cell biology of acute itch. *J Cell Biol*. 2016;213(2):155–161.
- LaMotte RH, Dong X, Ringkamp M. Sensory neurons and circuits mediating itch. *Nat Rev Neurosci*. 2014;15(1):19–31.
- Horsmanheimo L, Harvima IT, Harvima RJ, Brummer-Korvenkontio H, François G, Reunala T. Histamine and leukotriene C4 release in cutaneous mosquito-bite reactions. *J Allergy Clin Immunol*. 1996;98(2):408–411.
- McCoy ES, Taylor-Blake B, Street SE, Pribisko AL, Zheng J, Zylka MJ. Peptidergic CGRP α primary sensory neurons encode heat and itch and tonically suppress sensitivity to cold. *Neuron*. 2013;78(1):138–151.
- Simone DA, Ngeow JY, Whitehouse J, Becerra-Cabal L, Putterman GJ, LaMotte RH. The magnitude and duration of itch produced by intracutaneous injections of histamine. *Somatosens Res*. 1987;5(2):81–92.
- Dong X, Han S, Zylka MJ, Simon MI, Anderson DJ. A diverse family of GPCRs expressed in specific subsets of nociceptive sensory neurons. *Cell*. 2001;106(5):619–632.
- Han L, et al. A subpopulation of nociceptors specifically linked to itch. *Nat Neurosci*. 2013;16(2):174–182.
- Liu Q, et al. Sensory neuron-specific GPCR Mrgprs are itch receptors mediating chloroquine-induced pruritus. *Cell*. 2009;139(7):1353–1365.
- Meixiong J, Dong X. Mas-related G protein-coupled receptors and the biology of itch sensation. *Annu Rev Genet*. 2017;51:103–121.
- Imamachi N, et al. TRPV1-expressing primary afferents generate behavioral responses to pruritogens via multiple mechanisms. *Proc Natl Acad Sci U S A*. 2009;106(27):11330–11335.
- Kim S, et al. Facilitation of TRPV4 by TRPV1 is required for itch transmission in some sensory neuron populations. *Sci Signal*. 2016;9(437):ra71.
- Morita T, et al. HTR7 mediates serotonergic acute and chronic itch. *Neuron*. 2015;87(1):124–138.
- Wilson SR, Bautista DM. Role of transient receptor potential channels in acute and chronic itch. In: Carstens E, Akiyama T, eds. *Itch: Mechanisms and Treatment*. Boca Raton, Florida, USA: CRC Press; 2014:chapter 16.
- Wilson SR, et al. The ion channel TRPA1 is required for chronic itch. *J Neurosci*. 2013;33(22):9283–9294.
- Zhao ZQ, et al. Chronic itch development in sensory neurons requires BRAF signaling pathways. *J Clin Invest*. 2013;123(11):4769–4780.
- Ahern CA, Payandeh J, Bosmans F, Chanda B. The hitchhiker's guide to the voltage-gated sodium channel galaxy. *J Gen Physiol*. 2016;147(1):1–24.
- Dib-Hajj SD, Cummins TR, Black JA, Waxman SG. Sodium channels in normal and pathological pain. *Annu Rev Neurosci*. 2010;33:325–347.
- Faber CG, et al. Gain-of-function Nav1.8 mutations in painful neuropathy. *Proc Natl Acad Sci U S A*. 2012;109(47):19444–19449.
- Habib AM, Wood JN, Cox JJ. Sodium channels and pain. *Handb Exp Pharmacol*. 2015;227:39–56.
- Han C, et al. Familial gain-of-function Nav1.9 mutation in a painful channelopathy. *J Neurol Neurosurg Psychiatry*. 2017;88(3):233–240.
- Leipold E, et al. A de novo gain-of-function mutation in SCN11A causes loss of pain perception. *Nat Genet*. 2013;45(11):1399–1404.
- Leo S, D'Hooge R, Meert T. Exploring the role of nociceptor-specific sodium channels in pain transmission using Nav1.8 and Nav1.9 knockout mice. *Behav Brain Res*. 2010;208(1):149–157.
- Lolignier S, et al. The Nav1.9 channel is a key determinant of cold pain sensation and cold allodynia. *Cell Rep*. 2015;11(7):1067–1078.
- Priest BT, et al. Contribution of the tetrodotoxin-resistant voltage-gated sodium channel Nav1.9 to sensory transmission and nociceptive behavior. *Proc Natl Acad Sci U S A*. 2005;102(26):9382–9387.
- Cox JJ, et al. An SCN9A channelopathy causes congenital inability to experience pain. *Nature*. 2006;444(7121):894–898.
- Fertleman CR, et al. SCN9A mutations in paroxysmal extreme pain disorder: allelic variants underlie distinct channel defects and phenotypes. *Neuron*. 2006;52(5):767–774.
- Huang J, et al. Sodium channel Nav1.9 mutations associated with insensitivity to pain dampen neuronal excitability. *J Clin Invest*. 2017;127(7):2805–2814.
- Dib-Hajj SD, Black JA, Waxman SG. Nav1.9: a sodium channel linked to human pain. *Nat Rev Neurosci*. 2015;16(9):511–519.
- Leipold E, et al. Cold-aggravated pain in humans caused by a hyperactive Nav1.9 channel mutant. *Nat Commun*. 2015;6:10049.
- Woods CG, Babiker MO, Horrocks I, Tolmie J, Kurth I. The phenotype of congenital insensitivity to pain due to the Nav1.9 variant p.L811P. *Eur J Hum Genet*. 2015;23(10):1434.
- Ho TW, Backonja M, Ma J, Leibensperger H, Froman S, Polydefkis M. Efficient assessment of neuropathic pain drugs in patients with small fiber sensory neuropathies. *Pain*. 2009;141(1–2):19–24.
- Garcia-Borreguero D, Larrosa O, de la Llave Y, Verger K, Masramon X, Hernandez G. Treatment of restless legs syndrome with gabapentin: a double-blind, cross-over study. *Neurology*. 2002;59(10):1573–1579.
- Pédélec JD, Cabantous S, Tran T, Terwilliger TC, Waldo GS. Engineering and characterization of a superfolder green fluorescent protein. *Nat Biotechnol*. 2006;24(1):79–88.
- Lee A, Goldin AL. Role of the terminal domains in sodium channel localization. *Channels (Austin)*. 2009;3(3):171–180.
- Hershberg R, Petrov DA. Selection on codon bias. *Annu Rev Genet*. 2008;42:287–299.
- Tanaka KF, et al. Flexible Accelerated STOP Tetracycline operator-knockin (FAST): a versatile and efficient new gene modulating system. *Biol Psychiatry*. 2010;67(8):770–773.
- Hockley JR, et al. Multiple roles for Nav1.9 in the activation of visceral afferents by noxious inflammatory, mechanical, and human disease-derived stimuli. *Pain*. 2014;155(10):1962–1975.
- Maingret F, et al. Inflammatory mediators increase Nav1.9 current and excitability in nociceptors through a coincident detection mechanism. *J Gen Physiol*. 2008;131(3):211–225.
- Ostman JA, Nassar MA, Wood JN, Baker MD. GTP up-regulated persistent Na⁺ current and enhanced nociceptor excitability require Nav1.9.

- J Physiol (Lond)*. 2008;586(4):1077–1087.
41. Padilla F, et al. Expression and localization of the Nav1.9 sodium channel in enteric neurons and in trigeminal sensory endings: implication for intestinal reflex function and orofacial pain. *Mol Cell Neurosci*. 2007;35(1):138–152.
42. Vanoye CG, Ehring GR, George AL. Functional analysis of stably expressed human Nav1. *Biophys J*. 2012;102:527a.
43. Bosmans F, Puopolo M, Martin-Eauclaire MF, Bean BP, Swartz KJ. Functional properties and toxin pharmacology of a dorsal root ganglion sodium channel viewed through its voltage sensors. *J Gen Physiol*. 2011;138(1):59–72.
44. Nott A, Meislin SH, Moore MJ. A quantitative analysis of intron effects on mammalian gene expression. *RNA*. 2003;9(5):607–617.
45. Dib-Hajj SD, Tyrrell L, Escayg A, Wood PM, Meisler MH, Waxman SG. Coding sequence, genomic organization, and conserved chromosomal localization of the mouse gene *Scn11a* encoding the sodium channel NaN. *Genomics*. 1999;59(3):309–318.
46. Zhou X, et al. Electrophysiological and pharmacological analyses of Nav1.9 voltage-gated sodium channel by establishing a heterologous expression system. *Front Pharmacol*. 2017;8:852.
47. Amaya F, et al. The voltage-gated sodium channel Na(v)1.9 is an effector of peripheral inflammatory pain hypersensitivity. *J Neurosci*. 2006;26(50):12852–12860.
48. Caterina MJ, et al. Impaired nociception and pain sensation in mice lacking the capsaicin receptor. *Science*. 2000;288(5464):306–313.
49. Flatmark T. Catecholamine biosynthesis and physiological regulation in neuroendocrine cells. *Acta Physiol Scand*. 2000;168(1):1–17.
50. Brumovsky PR. Dorsal root ganglion neurons and tyrosine hydroxylase—an intriguing association with implications for sensation and pain. *Pain*. 2016;157(2):314–320.
51. Gautron L, Sakata I, Udit S, Zigman JM, Wood JN, Elmquist JK. Genetic tracing of Nav1.8-expressing vagal afferents in the mouse. *J Comp Neurol*. 2011;519(15):3085–3101.
52. Ross SE, et al. Loss of inhibitory interneurons in the dorsal spinal cord and elevated itch in *Bhlhb5* mutant mice. *Neuron*. 2010;65(6):886–898.
53. Ross SE, et al. *Bhlhb5* and *Prdm8* form a repressor complex involved in neuronal circuit assembly. *Neuron*. 2012;73(2):292–303.
54. Han L, et al. *Mrgpr*s on vagal sensory neurons contribute to bronchoconstriction and airway hyper-responsiveness. *Nat Neurosci*. 2018;21(3):324–328.
55. Azimi E, Reddy VB, Pereira PJS, Talbot S, Woolf CJ, Lerner EA. Substance P activates Mas-related G protein-coupled receptors to induce itch. *J Allergy Clin Immunol*. 2017;140(2):447–453.e3.
56. Maruyama H, et al. Electrophysiological characterization of the tetrodotoxin-resistant Na⁺ channel, Na(v)1.9, in mouse dorsal root ganglion neurons. *Pflugers Arch*. 2004;449(1):76–87.
57. Devigili G, et al. Paroxysmal itch caused by gain-of-function Nav1.7 mutation. *Pain*. 2014;155(9):1702–1707.